Aerospace Science and Technology 33 (2014) 122–134

Contents lists available at ScienceDirect

Aerospace Science and Technology

www.elsevier.com/locate/aescte

Strapdown stellar-inertial guidance system for launch vehicle

Lijun Zhang [a,*,1], Huabo Yang [a,2], Shifeng Zhang [a,3], Hong Cai [a,4], Shan Qian [b,5]

[a] College of Aerospace Science and Engineering, National University of Defense Technology, Changsha, 410073, China
[b] The State Key Laboratory of Astronautic Dynamics, China Xi'an Satellite Control Center, Xi'an, 710043, China

ARTICLE INFO

Article history:
Received 18 December 2012
Received in revised form 20 January 2014
Accepted 21 January 2014
Available online 27 January 2014

Keywords:
Responsive launch
Stellar-inertial guidance
Dual star correction
Gravity compensation

ABSTRACT

In this paper, a novel strapdown stellar-inertial guidance scheme is developed to correct the velocity and position navigation errors for responsive launch vehicle. Three types of error sources consisting of initial localization and misorientation errors, inertial sensor errors and gravity computation errors due to position navigation errors are discussed. The digital platform error model arising from initial localization and misorientation errors and gyro measurement error is derived. The detailed analysis for the velocity and position navigation errors caused by initial position errors, digital platform errors, accelerometer measurement error and gravity computation errors is performed. For the gravity computation errors due to the position navigation errors, an effective first-order approximation compensation scheme is addressed. A dual star correction strategy scheme is presented to estimate the error parameters and correct the cumulative velocity and position navigation errors. Compared with traditional stellar-inertial guidance algorithm based on nominal trajectory data and priori subsystem error statistics, the proposed algorithm uses the real-time trajectory data to calculate the function matrices used in the navigation error propagation equations. Thus, the corrections for velocity and position navigation errors are provided by the stringent navigation error model rather than the statistics of the subsystem errors caused by individual error source. Numerical examples are given to analyze the effects of the individual error factor with respect to the accuracy of strapdown INS and compare the navigation performances for all-inertial, stellar-inertial, and stellar-inertial plus gravity compensation guidance schemes.

1. Introduction

The keystone of the operationally responsive space (ORS) concept is a responsive launch capability [1]. Responsive launch specifies the reduction of launch-vehicle call-up times from months to days and of final preparation and launch from days to hours, which offers the potentially capability to inject the payload into orbit in several hours. One of the key technologies for responsive launch is the high-precision navigation and guidance technique. Several typical navigation systems used on launch vehicles include inertial navigation system (INS), radio navigation system, global navigation satellite system (GNSS) and celestial navigation system (CNS). An INS is a self-contained autonomous navigation system which uses gyroscopes and accelerometers to provide attitude information in addition to position and velocity. However, INS's rely on the availability of accurate knowledge of the initial state, and the accumulated navigation errors grow without bound due to the inertial sensor errors. Therefore, the integrated guidance schemes are usually used to improve the guidance accuracy, and two typical schemes are the integrated INS/GNSS and INS/CNS schemes. An integrated INS/GNSS uses an optimal estimator to fuse the GNSS and INS positioning and navigation information to yield a reliable navigation solution. But this integrated scheme is subject to the work performance of the satellites, and the high-precision attitude measurements from GNSS are still not available until now. In comparison with the INS/GNSS integration, an integrated INS/CNS scheme, also called as stellar-inertial guidance scheme, has the advantages of good automatic navigation and concealment performances as well as the capability to correct for the attitude errors.

Compared with all-inertial guidance systems, the major advantages of stellar-inertial guidance systems are quick reaction capability, the ability to correct for initial position and launch azimuth errors, and relatively low cost [11]. The basic principle of the stellar-inertial guidance system is to calibrate the inertial navigation system using the accurate orientation information provided by stellar sensor, which can relax the demands of localization and orientation for launch vehicle at launch and sequentially reduce the preparation time. It has been successfully applied in the submarine launched ballistic missile (SLBM) systems, such as Trident I

* Corresponding author.
E-mail addresses: alijun_007@163.com, alijun@nudt.edu.cn (L. Zhang), yhang0731@mailme.cn (H. Yang), zhang_shifeng@hotmail.com (S. Zhang), hcai@nudt.edu.cn (H. Cai), shanqian_123@163.com (S. Qian).
[1] Doctoral Student, Department of Astronautics Science & Engineering.
[2] Assistant Professor, Department of Astronautics Science & Engineering.
[3] Professor, Department of Astronautics Science & Engineering.
[4] Professor, Department of Astronautics Science & Engineering.
[5] Aerospace Engineer.

1270-9638/$ – see front matter
http://dx.doi.org/10.1016/j.ast.2014.01.007

Nomenclature

ORS	operationally responsive space
SLBM	submarine launched ballistic missile
INS	inertial navigation system
GNSS	global navigation satellite system
CNS	celestial navigation system
ECEF	Earth-Centered-Earth-Fixed (E-frame)
LCI	Launch-Centered-Inertial (I-frame)
LCEF	Launch-Centered-Earth-Fixed (G-frame)
DCM	direction cosine matrix
EKF	extended Kalman filter
$(\boldsymbol{M}_1[\cdot], \boldsymbol{M}_2[\cdot], \boldsymbol{M}_3[\cdot])$	attitude transformation matrices rotating about x, y, z axes, respectively
$\boldsymbol{I}_{3\times3}$	3×3 identity matrix
$(A_0, B_0, \lambda_0, h_0)$	nominal launch azimuth, latitude, longitude, and height of launch site
$(\Delta A_0, \Delta B_0, \Delta\lambda_0)$	initial launch azimuth, latitude and longitude errors
$\boldsymbol{\Delta}$	initial localization and misorientation error vector
$\boldsymbol{\alpha}_\Delta$	initial digital platform error caused by the initial localization and misorientation errors
$\boldsymbol{\alpha}_g$	digital platform error caused by the gyro measurement error
$\boldsymbol{\alpha}$	total misalignment angle or digital platform error vector
$\boldsymbol{\omega}_{B/I}^B$	angular velocity vector
$\delta\boldsymbol{\omega}_{B/I}^B$	gyro measurement error
$\boldsymbol{D}_g$	gyro error coefficients
$\delta\boldsymbol{f}^B$	accelerometer measurement error
$\boldsymbol{D}_a$	accelerometer error coefficients
$\Delta\boldsymbol{r}_0$	initial position navigation error
$\Delta\boldsymbol{v}_0$	initial velocity navigation error
$\dot{\boldsymbol{W}}^B$	output apparent acceleration expressed in the body frame
$\dot{\boldsymbol{W}}^I$	true apparent acceleration expressed in the I frame
$\Delta\dot{\boldsymbol{W}}^I$	apparent acceleration measurement error
$\Delta\boldsymbol{W}^I$	apparent velocity navigation error
$\Delta\boldsymbol{r}^I$	apparent position navigation error
$\Delta\boldsymbol{g}^I$	gravity computation error due to the position navigation errors
$\boldsymbol{X}^I$	navigation position vector expressed in the theory LCI frame
$\boldsymbol{X}^{I'}$	true position vector expressed in the actual LCI frame
$\boldsymbol{\rho}_o^I$	position vector from the Earth center to the nominal launch site expressed in the theory LCI frame
$\boldsymbol{\rho}_{o'}^{I'}$	position vector from the Earth center to the actual launch site expressed in the actual LCI frame
$\Delta\boldsymbol{v}_g$	velocity navigation error due to the gravity computation errors
$\Delta\boldsymbol{r}_g$	position navigation error due to the gravity computation errors
$\Delta\boldsymbol{v}$	total velocity navigation errors
$\Delta\boldsymbol{r}$	total position navigation errors
t	flight time, $t_0 = 0$
t_k	shut down time
$E\{\cdot\}$	expectation
ω_e	earth rotation rate
e	earth eccentricity
$\hat{\boldsymbol{\alpha}}_k$	estimate of the digital platform misalignment angle at shut down time t_k
$\hat{\boldsymbol{\alpha}}_0$	estimate of the initial digital platform misalignment angle
$(\boldsymbol{\eta}_\omega, \boldsymbol{\eta}_a, \boldsymbol{\eta}_s)$	gyro, accelerometer and star sensor measurement noises, respectively
$(\sigma_\omega, \sigma_a, \sigma_s)$	gyro, accelerometer and star sensor measurement noise strengths, respectively

missile of America [20], and SS-N-8, SS-N-18 and SS-N-20 missiles of Soviet Union [4]. In view of the similarity of launch vehicle and ballistic missile, the stellar-inertial guidance scheme is introduced into launch vehicles to satisfy the requirements of responsive launch.

In terms of the mounting position of the inertial sensors, the INS's are typically divided into gimbaled INS and strapdown INS. In the gimbaled INS, the inertial sensors are mounted on a stable platform which is stabilized in space, while in the strapdown INS, the inertial sensors are directly mounted on the vehicle [19]. Therefore, the corresponding stellar-inertial guidance systems fall into gimbaled and strapdown stellar-inertial systems. For a gimbaled system, the stellar sensor is mounted with the inertial platform and the inertial reference frame is maintained by cluster; while for a strapdown system, the stellar sensor is integrally mounted with vehicle itself and the inertial reference frame is maintained by the flight computer software. Actually, many concepts discussed in these two stellar-inertial guidance systems are not different, and the most significant difference lies in the mechanization of the stellar sighting itself [11]. Although the strapdown INS is not comparable to gimbaled INS in the degree of accuracy presently, it has obvious advantages in the flexibility and cost which satisfy the requirements of responsive launch. Therefore, strapdown stellar-inertial guidance scheme has become an important research direction in the inertial guidance area.

In the early open literature, only the basic principle of the stellar-inertial guidance system was introduced, but the detailed models and methods were not discussed [11,7,6,5]. For the gimbaled stellar-inertial system, a single-star scheme has been presented in [2]. In recent years, Zhang et al. further presented the concept of equivalent information compression to explain the implementation principle of the single-star stellar-inertial guidance technique [25] and studied the application of this guidance scheme to responsive launch vehicle [24]. However, in [24], only the positioning and orientation errors but no inertial sensor errors were taken into consideration. In addition, the analysis of the error factors affecting the INS and the correction scheme were not discussed in depth. For the strapdown stellar-inertial system, an integrated INS/CNS navigation algorithm using the neural network Kalman filter was addressed by Xu and Fang [23] and a strapdown inertial/starlight integrated guidance scheme for ballistic missiles was presented by Wang [22]. In [23], the prelaunch position and azimuth uncertainties which are essentially the primary error sources resulting in the velocity and position navigation errors during the boost phase were not considered. In [22], the prelaunch azimuth errors were not considered, and the effects of the prelaunch position errors with respect to navigation computation frame were not analyzed. Unfortunately, in both references, the computations for the error propagation transition matrix, which are used to correct the cumulative velocity and position navigation errors, were vague and cumbersome.

In this paper, three types of error sources affecting the strapdown INS are discussed in detail. They are initial localization and misorientation errors (i.e. prelaunch position and azimuth errors), inertial sensor errors and the gravity computation errors due to the position navigation errors. The inertial sensor errors are referred

to as gyro and accelerometer sensor errors. A more general inertial sensor error model including drifts, scale factors, misalignments and measurement noises is used [10,8]. The principal software functions executed in the strapdown INS computer (i.e., digital platform) are the integration of angular rate into attitude, acceleration transformation and integration into velocity, and integration of velocity into position [12]. Due to the initial localization and misorientation errors as well as gyro measurement error, there exist misalignment errors between the computation frame and navigation frame which are called as digital platform errors. It is evident that the velocity and position navigation results are affected by digital platform errors, initial position errors and accelerometer measurement error. Besides, since the gravitation acceleration is computed using the navigation information, there are computation errors in the gravity computation due to the position navigation errors, which consists of initial position errors and cumulative position errors during the boosted flight. The navigation accuracy can be improved if this type of error source compensated, particular for the velocity navigation result. Since the flight time is not long, the navigation errors caused by inertial sensors are generally not large and the initial localization and misorientation errors are the primary error factors resulting in the navigation errors among others. Therefore, it is necessary to decrease the prelaunch position and azimuth errors if possible.

Traditional stellar-inertial guidance algorithm [11,5], which uses a precomputed (9×2) gain matrix to correct the nine components of position and velocity as well as attitude or a 2×2 matrix to correct down-range and cross-range miss directly, is based on the nominal trajectory data and priori subsystem error statistics. When the INS is affected by more than one type of error source, in general, not the perfect coefficients but merely the statistically optimal weighting coefficients can be calculated a priori. In order to solve this problem, this paper performs a detailed analysis of the mentioned three types of error source behaviors as applied to launch vehicle flight, and presents a dual star correction strategy scheme to estimate the error parameters and correct the cumulative velocity and position navigation errors. In this stellar-inertial guidance scheme, the function matrices used in the navigation error propagation equations are computed by using the real-time flight data rather than the nominal trajectory data, and the selection of the optimal stellar sighting direction does not need to be considered.

This paper is outlined as follows. In Section 2, the various reference frames used in stellar-inertial guidance system are firstly summarized. Then, a detailed analysis for digital platform errors resulting from prelaunch position and azimuth errors as well as gyro measurement error is performed, and the stringent digital platform error model is formulated. Section 3 derives a detailed mathematics model for navigation errors caused by initial position errors, digital platform errors, accelerometer measurement error, and gravity computation errors due to the position navigation errors. A compensation scheme for the gravity computation errors due to the position navigation errors is addressed. In Section 4, a dual star correction strategy scheme is presented to estimate the error parameters and correct for the cumulative velocity and position navigation errors. In Section 5, simulation results are presented that analyze the effects of the individual error factor with respect to strapdown INS and compare the navigation performances for all-inertial, stellar-inertial, and stellar-inertial plus gravity compensation guidance schemes.

2. Reference frames and digital platform error analysis

2.1. Reference frames

In this section the reference frames used in this paper are summarized, as shown in Fig. 1:

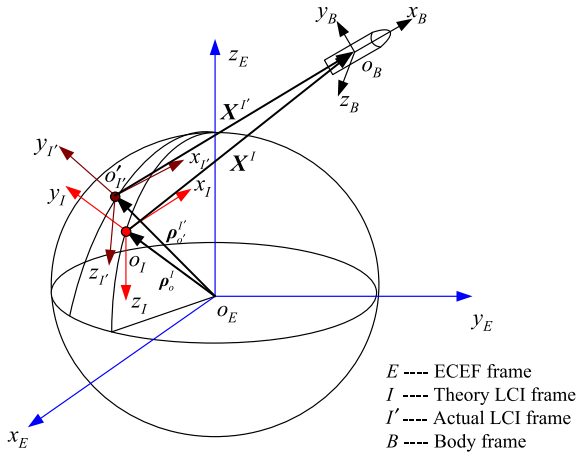

Fig. 1. Definitions of various reference frames.

(1) Earth-Centered-Earth-Fixed (ECEF) Frame (E-frame): The frame has its origin at the center of the Earth and axes which are fixed with respect to the Earth. The z axis points in the direction of the North pole, the x axis points in the direction of the Earth's prime meridian, and the y axis completes the right-handed system.

(2) Launch-Centered-Inertial (LCI) Frame (I-frame): The frame is inertially fixed and is centered at launch site at the instant of launch. In this system, the x axis is taken to be in the horizontal plane and in the direction of launch, the positive y axis vertical, and the z axis completing the right-handed coordinate system.

(3) Launch-Centered-Earth-Fixed (LCEF) Frame (G-frame): This is an Earth-fixed coordinate system, having the same orientation as the LCI frame.

(4) Navigation Computation Frame (P-frame): In a strapdown system, the frame is a virtual digital platform frame which has its origin at the location of strapdown INS and axes aligned with the directions of LCI frame.

(5) Body Frame (B-frame): This frame is fixed onto the vehicle body and rotates with it. The positive x axis coincides with the vehicle's center line or longitudinal axis. The positive z axis is to the right of the x axis in the horizontal plane and designated as pitch axis. The y axis is the yaw axis and completes the right-handed system.

Herein two LCI frames are defined, one is the theory LCI frame (I-frame), and the other is the actual LCI frame (I'-frame). The theory LCI frame is established on the nominal launch site and is referred to as guidance frame stored in the navigation computer, while the actual LCI frame is established on the actual launch site. Since the prelaunch position and azimuth are with errors, there are the misorientation errors between the theory and actual LCI frames. During the actual flight, the gyro measurement error also leads to the misorientation errors between the navigation computation frame (P-frame) and theory LCI frame (I-frame). Therefore, there exist misalignment errors between the P frame and the I frame, which are called as digital platform errors. For small angles of misalignment, the misalignment of the P frame relative to the I frame can be described using misalignment angle $\boldsymbol{\alpha}$ as [16]

$$\boldsymbol{R}_I^P = \boldsymbol{I}_{3\times 3} - [\boldsymbol{\alpha}\times] \tag{1}$$

where $\boldsymbol{I}_{3\times 3}$ is a 3×3 identity matrix, $[\boldsymbol{\alpha}\times]$ is a cross product matrix defined by

$$[\boldsymbol{\alpha}\times] \equiv \begin{bmatrix} 0 & -\alpha_z & \alpha_y \\ \alpha_z & 0 & -\alpha_x \\ -\alpha_y & \alpha_x & 0 \end{bmatrix} \tag{2}$$

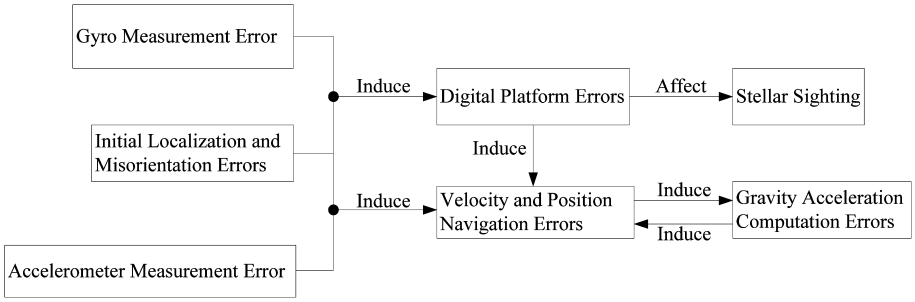

Fig. 2. Navigation error analysis of strapdown inertial navigation system.

The main error factors affecting the inertial navigation results include initial localization and misorientation errors (i.e. prelaunch position and azimuth errors) and inertial sensor errors. The inertial sensor errors are referred to as gyro and accelerometer measurement errors. The effects of the initial localization and misorientation errors are divided into two parts: one part is to induce the digital platform errors, and the other part is to induce the initial velocity and position navigation errors. As mentioned above, the digital platform errors are caused by the initial localization and misorientation errors and gyro measurement error. The stellar update algorithm uses the star sensor measurements to estimate the digital platform errors. Obviously, the velocity and position navigation errors are caused by digital platform errors, initial localization and misorientation errors as well as accelerometer measurement error. In addition, the gravitational acceleration computation errors due to the position navigation errors also cause velocity and position navigation error, and the navigation accuracy can be further improved if these errors compensated. Therein-after, the digital platform errors are discussed in detail and the detailed analysis for the navigation errors will be performed in Section 3. Fig. 2 shows the navigation error analysis of strapdown INS.

2.2. Digital platform errors caused by initial localization and misorientation errors

Since the LCI frame coincides with the LCEF frame at the instant of launch, the initial ECEF-to-LCI attitude matrix equals the ECEF-to-LCEF attitude matrix, that is [18]

$$\boldsymbol{R}_E^I(0) = \boldsymbol{R}_E^G = \boldsymbol{M}_2\big[-(90^\circ + A_0)\big]\boldsymbol{M}_1[B_0]\boldsymbol{M}_3[\lambda_0 - 90^\circ] \tag{3}$$

where A_0, B_0, λ_0 are the nominal launch azimuth, latitude and longitude of launch site, respectively; $\boldsymbol{M}_1[\cdot]$, $\boldsymbol{M}_2[\cdot]$, $\boldsymbol{M}_3[\cdot]$ are the attitude transformation matrices rotating about x, y, z axes, respectively.

Considering the effects of the initial localization and misorientation errors, the direction cosine matrix (DCM) relating the ECEF frame and the actual LCI frame is given by

$$\begin{aligned}\boldsymbol{R}_E^{I'}(0) = {} & \boldsymbol{M}_2\big[-(90^\circ + A_0 + \Delta A_0)\big]\boldsymbol{M}_1[B_0 + \Delta B_0] \\ & \times \boldsymbol{M}_3[\lambda_0 + \Delta\lambda_0 - 90^\circ]\end{aligned} \tag{4}$$

where ΔA_0, ΔB_0, $\Delta\lambda_0$ are the launch azimuth, latitude and longitude errors, respectively. These errors can be described in vector form as $\boldsymbol{\Delta} = [\Delta A_0 \ \Delta B_0 \ \Delta\lambda_0]^{\mathrm{T}}$.

By using Eqs. (3) and (4) and first-order approximation, we obtain

$$\begin{aligned}\boldsymbol{R}_I^{I'} &= \boldsymbol{R}_E^{I'}(0)\boldsymbol{R}_I^E(0) \\ &= \begin{bmatrix} 1 & -\Delta B_0\cos A_0 - \Delta\lambda_0 \sin A_0 \cos B_0 & (\Delta A_0 - \Delta\lambda_0 \sin B_0) \\ \Delta B_0 \cos A_0 + \Delta\lambda_0 \sin A_0 \cos B_0 & 1 & (\Delta\lambda_0 \cos A_0 \cos B_0 - \Delta B_0 \sin A_0) \\ -(\Delta A_0 - \Delta\lambda_0 \sin B_0) & -(\Delta\lambda_0 \cos A_0 \cos B_0 - \Delta B_0 \sin A_0) & 1 \end{bmatrix}\end{aligned} \tag{5}$$

where $\boldsymbol{R}_I^E(0)$ is the transpose matrix of $\boldsymbol{R}_E^I(0)$. Since the theory and actual LCI frames are both inertial reference frames, the attitude error matrix $\boldsymbol{R}_I^{I'}$ does not change with time. For small angles of attitude errors, the attitude error matrix also can be expressed as

$$\boldsymbol{R}_I^{I'} = \boldsymbol{I}_{3\times 3} - [\boldsymbol{\alpha}_\Delta \times] \tag{6}$$

where $\boldsymbol{\alpha}_\Delta$ is the initial digital platform error caused by the initial localization and misorientation errors.

Comparing Eqs. (5) and (6) yields

$$\begin{aligned}\boldsymbol{\alpha}_\Delta &= \begin{bmatrix} \alpha_{\Delta x} \\ \alpha_{\Delta y} \\ \alpha_{\Delta z} \end{bmatrix} = \begin{bmatrix} 0 & -\sin A_0 & \cos A_0 \cos B_0 \\ -1 & 0 & \sin B_0 \\ 0 & -\cos A_0 & -\sin A_0 \cos B_0 \end{bmatrix} \begin{bmatrix} \Delta A_0 \\ \Delta B_0 \\ \Delta\lambda_0 \end{bmatrix} \\ &\triangleq \boldsymbol{N}_\Delta \boldsymbol{\Delta}\end{aligned} \tag{7}$$

It is shown from Eq. (7) that the determinant of $\boldsymbol{N}_\Delta$ is $\cos B_0$. In general, the latitude of launch site is not equal to 90° or -90° and thus the matrix $\boldsymbol{N}_\Delta$ can be inversed. Therefore, the initial localization and misorientation errors $\boldsymbol{\Delta}$ can be uniquely determined when obtaining $\boldsymbol{\alpha}_\Delta$.

2.3. Digital platform errors caused by gyro measurement error

Since the LCI frame is selected as the navigation frame, the attitude kinematics equation is given by [15]

$$\dot{\boldsymbol{R}}_B^I = \boldsymbol{R}_B^I\big[\boldsymbol{\omega}_{B/I}^B \times\big] \tag{8}$$

where $\boldsymbol{R}_B^I$ is the transformation matrix from the B frame to the I frame and $\boldsymbol{\omega}_{B/I}^B$ is angular velocity of the B frame relative to the I frame expressed in the B coordinates.

When computing the attitude matrix $\boldsymbol{R}_B^I$, the actual computation result contains the error term $\delta\boldsymbol{R}_B^I$ since the output angular velocity is contaminated by the gyro measurement error. Thus, the actual computation result $\tilde{\boldsymbol{R}}_B^I$ is given by

$$\tilde{\boldsymbol{R}}_B^I = \boldsymbol{R}_B^I + \delta\boldsymbol{R}_B^I \tag{9}$$

In fact, the navigation computation result $\tilde{\boldsymbol{R}}_B^I$ is equivalent to the attitude matrix $\boldsymbol{R}_B^P$ provided by strapdown INS which maps the B frame to the P frame, which can be expressed as

$$\tilde{\boldsymbol{R}}_B^I = \boldsymbol{R}_B^P = \boldsymbol{R}_I^P \boldsymbol{R}_B^I = \big(\boldsymbol{I}_{3\times 3} - [\boldsymbol{\alpha}\times]\big)\boldsymbol{R}_B^I \tag{10}$$

Comparing Eqs. (9) and (10) gives

$$\delta\boldsymbol{R}_B^I = -[\boldsymbol{\alpha}\times]\boldsymbol{R}_B^I \tag{11}$$

By differentiating Eq. (11) and using Eq. (8), we have

$$\begin{aligned}\delta\dot{\boldsymbol{R}}_B^I &= -[\dot{\boldsymbol{\alpha}}\times]\boldsymbol{R}_B^I - [\boldsymbol{\alpha}\times]\dot{\boldsymbol{R}}_B^I \\ &= -[\dot{\boldsymbol{\alpha}}\times]\boldsymbol{R}_B^I - [\boldsymbol{\alpha}\times]\boldsymbol{R}_B^I\big[\boldsymbol{\omega}_{B/I}^B \times\big]\end{aligned} \tag{12}$$

On the other hand, taking the perturbation on the both sides of Eq. (8) and using Eq. (11) yields

$$\begin{aligned}\delta\dot{\boldsymbol{R}}_B^I &= \delta\boldsymbol{R}_B^I\big[\boldsymbol{\omega}_{B/I}^B\times\big] + \boldsymbol{R}_B^I\big[\delta\boldsymbol{\omega}_{B/I}^B\times\big] \\ &= -[\boldsymbol{\alpha}\times]\boldsymbol{R}_B^I\big[\boldsymbol{\omega}_{B/I}^B\times\big] + \boldsymbol{R}_B^I\big[\delta\boldsymbol{\omega}_{B/I}^B\times\big]\end{aligned} \tag{13}$$

Equating Eqs. (12) and (13) gives

$$[\dot{\boldsymbol{\alpha}}\times] = -\boldsymbol{R}_B^I\big[\delta\boldsymbol{\omega}_{B/I}^B\times\big]\boldsymbol{R}_I^B \tag{14}$$

where $\boldsymbol{R}_I^B$ is the transpose matrix of $\boldsymbol{R}_B^I$ and $\delta\boldsymbol{\omega}_{B/I}^B$ is the gyro measurement error.

Rearranging Eq. (14) gives the following vector form

$$\dot{\boldsymbol{\alpha}} = -\boldsymbol{R}_B^I\delta\boldsymbol{\omega}_{B/I}^B \tag{15}$$

Therefore, we obtain the digital platform error by taking the integral of $\dot{\boldsymbol{\alpha}}$ over time. Mathematically,

$$\boldsymbol{\alpha} = \boldsymbol{\alpha}|_{t=0} - \int_0^t \boldsymbol{R}_B^I\delta\boldsymbol{\omega}_{B/I}^B\,dt \tag{16}$$

where t is the flight time. From the previous analysis, it can be seen that the digital platform error at time $t=0$ is essentially the misalignment error of the I' frame relative to the I frame. Thus, Eq. (16) becomes

$$\boldsymbol{\alpha} = \boldsymbol{\alpha}_\Delta + \boldsymbol{\alpha}_g \tag{17}$$

where $\boldsymbol{\alpha}_g = -\int_0^t \boldsymbol{R}_B^I\delta\boldsymbol{\omega}_{B/I}^B\,dt$ is defined as the digital platform error caused by the gyro measurement error.

The optic fiber gyro measurement error model is given by

$$\begin{aligned}\delta\boldsymbol{\omega}_{B/I}^B &= \begin{bmatrix} D_{0x} + D_{xx}\omega_x + D_{xy}\omega_y + D_{xz}\omega_z \\ D_{0y} + D_{yx}\omega_x + D_{yy}\omega_y + D_{yz}\omega_z \\ D_{0z} + D_{zx}\omega_x + D_{zy}\omega_y + D_{zz}\omega_z \end{bmatrix} + \boldsymbol{\eta}_\omega \\ &\triangleq \boldsymbol{N}_{gyro}\boldsymbol{D}_g + \boldsymbol{\eta}_\omega\end{aligned} \tag{18}$$

with

$$\boldsymbol{N}_{gyro} = \begin{bmatrix} 1 & \omega_x & \omega_y & \omega_z & 0 & 0 & 0 & 0 & 0 & 0 & 0 & 0 \\ 0 & 0 & 0 & 0 & 1 & \omega_x & \omega_y & \omega_z & 0 & 0 & 0 & 0 \\ 0 & 0 & 0 & 0 & 0 & 0 & 0 & 0 & 1 & \omega_x & \omega_y & \omega_z \end{bmatrix} \tag{19}$$

$$\boldsymbol{D}_g = [\,D_{0x}\;\; D_{xx}\;\; D_{xy}\;\; D_{xz}\;\; D_{0y}\;\; D_{yx}\;\; D_{yy}\;\; D_{yz}\;\; D_{0z}\;\; D_{zx}\;\; D_{zy}\;\; D_{zz}\,]^{\mathrm{T}} \tag{20}$$

where D_{0x}, D_{0y}, D_{0z} are the gyro drifts; D_{xx}, D_{yy}, D_{zz} are the scale factors; D_{xy}, D_{xz}, D_{yx}, D_{yz}, D_{zx}, D_{zy} are the misalignments. Measurement noise $\boldsymbol{\eta}_\omega$ is zero-mean Gaussian white-noise processes with spectral densities given by $\sigma_\omega^2\boldsymbol{I}_{3\times3}$.

Substituting Eq. (18) into the variable $\boldsymbol{\alpha}_g$ gives

$$\boldsymbol{\alpha}_g = -\int_0^t \boldsymbol{R}_B^I(\boldsymbol{N}_{gyro}\boldsymbol{D}_g + \boldsymbol{\eta}_\omega)\,dt \approx -\int_0^t \boldsymbol{R}_B^I\boldsymbol{N}_{gyro}\,dt\,\boldsymbol{D}_g \tag{21}$$

Since the true attitude matrix $\boldsymbol{R}_B^I$ is not available during the flight, Eq. (21) needs to be further rewritten by using the available navigation result $\boldsymbol{R}_B^P$ as

$$\begin{aligned}\boldsymbol{\alpha}_g &= -\int_0^t \big(\boldsymbol{I}_{3\times3} + [\boldsymbol{\alpha}\times]\big)\boldsymbol{R}_B^P\boldsymbol{N}_{gyro}\,dt\,\boldsymbol{D}_g \\ &= -\int_0^t \boldsymbol{R}_B^P\boldsymbol{N}_{gyro}\,dt\,\boldsymbol{D}_g + \int_0^t \big[\boldsymbol{R}_B^P\boldsymbol{N}_{gyro}\boldsymbol{D}_g\times\big]\boldsymbol{\alpha}\,dt \\ &\approx -\int_0^t \boldsymbol{R}_B^P\boldsymbol{N}_{gyro}\,dt\,\boldsymbol{D}_g \triangleq \boldsymbol{N}_g\boldsymbol{D}_g\end{aligned} \tag{22}$$

where $\boldsymbol{R}_B^P$ is the navigation computation result provided by strapdown INS. It can be seen from Eq. (22) that $\boldsymbol{\alpha}_g$ is an approximate linear function of $\boldsymbol{D}_g$. Furthermore, it follows from Eqs. (17), (7) and (22) that the term $\int_0^t[\boldsymbol{R}_B^P\boldsymbol{N}_{gyro}\boldsymbol{D}_g\times]\boldsymbol{\alpha}\,dt$ is a second-order small quantity and the approximation on the right side of Eq. (22) is reasonable. Since the true angular velocity is not available, the gyro measured rate is used to substitute for the true rate when computing matrix $\boldsymbol{N}_{gyro}$. In fact, the second-order error effect caused by this approximation can be neglected.

Inserting Eqs. (7) and (22) into Eq. (17), the total misalignment angles can be expressed as

$$\boldsymbol{\alpha} = \boldsymbol{N}_\alpha\cdot\boldsymbol{K} \tag{23}$$

with

$$\boldsymbol{N}_\alpha = [\,\boldsymbol{N}_\Delta \quad \boldsymbol{N}_g \quad 0_{3\times12}\,] \tag{24}$$

$$\boldsymbol{K} = \big[\,\boldsymbol{\Delta}^{\mathrm{T}} \quad \boldsymbol{D}_g^{\mathrm{T}} \quad \boldsymbol{D}_a^{\mathrm{T}}\,\big]^{\mathrm{T}} \tag{25}$$

where $\boldsymbol{K}$ is the error parameter vector to be determined, and $\boldsymbol{D}_a$ is the 12-dimension error coefficients of the accelerometers which will be defined in Section 3.

3. Navigation error analysis

In this section, a detailed analysis for the position and velocity navigation errors is performed and an effective compensation scheme for the gravity computation errors due to the position navigation errors is addressed. As illustrated in Fig. 2, the position and velocity navigation errors are caused by initial position errors, digital platform errors, accelerometer measurement error and gravity acceleration computation errors. The corresponding effects with respect to strapdown INS are discussed in the following context. In this paper, the navigation errors are defined as the errors that navigation position and velocity in the theory LCI frame minus true position and velocity in the theory LCI frame.

3.1. Navigation errors caused by initial position errors

The ECEF position coordinates of launch site are computed using [3]

$$\begin{aligned}x^E &= (N+h_0)\cos B_0\cos\lambda_0 \\ y^E &= (N+h_0)\cos B_0\sin\lambda_0 \\ z^E &= \big[N\big(1-e^2\big)+h_0\big]\sin B_0\end{aligned} \tag{26}$$

where B_0, λ_0, h_0 are latitude, longitude, height of launch site, and N is the length of the normal to the ellipsoid, given by

$$N = \frac{a}{\sqrt{1-e^2\sin^2 B_0}} \tag{27}$$

where $a = 6{,}378{,}137.0$ is the Earth semimajor axis and $e = 0.0818$ is the earth eccentricity.

Taking the partials of the quantities in Eq. (26) with respect to B_0, λ_0, and h_0, which leads to the following partial matrix [3]:

$$\boldsymbol{H}=\begin{bmatrix} \frac{\partial N}{\partial B_0}\cos B_0\cos\lambda_0-(N+h_0)\sin B_0\cos\lambda_0 & -(N+h_0)\cos B_0\sin\lambda_0 & \cos B_0\cos\lambda_0 \\ \frac{\partial N}{\partial B_0}\cos B_0\sin\lambda_0-(N+h_0)\sin B_0\sin\lambda_0 & (N+h_0)\cos B_0\cos\lambda_0 & \cos B_0\sin\lambda_0 \\ \frac{\partial N}{\partial B_0}(1-e^2)\sin B_0+[N(1-e^2)+h_0]\cos B_0 & 0 & \sin B_0 \end{bmatrix} \tag{28}$$

with

$$\frac{\partial N}{\partial B_0}=\frac{ae^2\sin B_0\cos B_0}{(1-e^2\sin^2 B_0)^{3/2}} \tag{29}$$

Since the height h_0 is generally measured exactly, the effect of height error can be ignored. Therefore, the ECEF position errors can be described by using initial localization and misorientation errors as

$$\begin{bmatrix}\Delta x^E\\ \Delta y^E\\ \Delta z^E\end{bmatrix} =\begin{bmatrix} 0 & \frac{\partial N}{\partial B_0}\cos B_0\cos\lambda_0-(N+h_0)\sin B_0\cos\lambda_0 & -(N+h_0)\cos B_0\sin\lambda_0 \\ 0 & \frac{\partial N}{\partial B_0}\cos B_0\sin\lambda_0-(N+h_0)\sin B_0\sin\lambda_0 & (N+h_0)\cos B_0\cos\lambda_0 \\ 0 & \frac{\partial N}{\partial B_0}(1-e^2)\sin B_0+[N(1-e^2)+h_0]\cos B_0 & 0 \end{bmatrix} \times\begin{bmatrix}\Delta A_0\\ \Delta B_0\\ \Delta\lambda_0\end{bmatrix}\triangleq\boldsymbol{\mathcal{H}}\boldsymbol{\Delta} \tag{30}$$

Since the navigation errors are defined in the theory LCI frame, the ECEF position errors are then transformed into the theory LCI frame, expressed as

$$\boldsymbol{r}^I_{0I'}=\boldsymbol{R}^I_E(0)\boldsymbol{\mathcal{H}}\boldsymbol{\Delta}\triangleq\boldsymbol{P}\boldsymbol{\Delta} \tag{31}$$

where $\boldsymbol{r}^I_{0I'}$ is the position of the actual launch site expressed in the theory LCI frame, which can be interpreted as the position errors between the nominal launch site and the actual launch site. Define $\boldsymbol{\rho}^I_o$ is the position vector from the Earth center to the nominal launch site expressed in the theory LCI frame and $\boldsymbol{\rho}^{I'}_{o'}$ is the position vector from the Earth center to the actual launch site expressed in the actual LCI frame. Therefore, $\boldsymbol{r}^I_{0I'}$ can be described as

$$\boldsymbol{r}^I_{0I'}=\boldsymbol{R}^I_{I'}\boldsymbol{\rho}^{I'}_{o'}-\boldsymbol{\rho}^I_o \tag{32}$$

By the definition of position navigation error, the initial position navigation error $\Delta\boldsymbol{r}_0$ is actually equal to $-\boldsymbol{r}^I_{0I'}$, that is

$$\Delta\boldsymbol{r}_0=\boldsymbol{\rho}^I_o-\boldsymbol{R}^I_{I'}\boldsymbol{\rho}^{I'}_{o'}=-\boldsymbol{P}\boldsymbol{\Delta} \tag{33}$$

By the definition of velocity navigation error, the initial velocity navigation error $\Delta\boldsymbol{v}_0$ is given by

$$\begin{aligned}\Delta\boldsymbol{v}_0&=\boldsymbol{\omega}^I_e\times\boldsymbol{\rho}^I_o-\boldsymbol{R}^I_{I'}\big(\boldsymbol{\omega}^{I'}_e\times\boldsymbol{\rho}^{I'}_{o'}\big)\\ &=\boldsymbol{\omega}^I_e\times\boldsymbol{\rho}^I_o-\big(\boldsymbol{R}^I_{I'}\boldsymbol{\omega}^{I'}_e\big)\times\big(\boldsymbol{R}^I_{I'}\boldsymbol{\rho}^{I'}_{o'}\big)\\ &=\big[\boldsymbol{\omega}^I_e\times\big]\big(\boldsymbol{\rho}^I_o-\boldsymbol{R}^I_{I'}\boldsymbol{\rho}^{I'}_{o'}\big)\end{aligned} \tag{34}$$

where $\boldsymbol{\omega}^I_e$ and $\boldsymbol{\omega}^{I'}_e$ are the earth rates expressed in the theory and actual LCI frames, respectively. Substituting Eq. (33) into Eq. (34) leads to

$$\Delta\boldsymbol{v}_0=-\big[\boldsymbol{\omega}^I_e\times\big]\boldsymbol{P}\boldsymbol{\Delta}\triangleq-\boldsymbol{Q}\boldsymbol{\Delta} \tag{35}$$

with

$$\boldsymbol{\omega}^I_e=\omega_e\begin{bmatrix}\cos B_0\cos A_0 & \sin B_0 & -\cos B_0\sin A_0\end{bmatrix}^{\mathrm{T}} \tag{36}$$

where ω_e is the Earth's rotation rate given as 7.292115×10^{-5} rad/s.

Hence, the initial position and velocity navigation errors can be described using the to-be-determined parameter vector $\boldsymbol{K}$ as

$$\Delta\boldsymbol{r}_0=\begin{bmatrix}-\boldsymbol{P} & \boldsymbol{0}_{3\times12} & \boldsymbol{0}_{3\times12}\end{bmatrix}\boldsymbol{K}\triangleq\boldsymbol{N}_{\boldsymbol{r}_0}\boldsymbol{K} \tag{37}$$

$$\Delta\boldsymbol{v}_0=\begin{bmatrix}-\boldsymbol{Q} & \boldsymbol{0}_{3\times12} & \boldsymbol{0}_{3\times12}\end{bmatrix}\boldsymbol{K}\triangleq\boldsymbol{N}_{\boldsymbol{v}_0}\boldsymbol{K} \tag{38}$$

3.2. Navigation errors caused by digital platform errors and accelerometer measurement error

The measurement error of the apparent acceleration, $\Delta\dot{\boldsymbol{W}}^I$, is expressed in the theory LCI frame as

$$\Delta\dot{\boldsymbol{W}}^I=\tilde{\dot{\boldsymbol{W}}}^I-\dot{\boldsymbol{W}}^I=\boldsymbol{R}^P_B\dot{\boldsymbol{W}}^B-\boldsymbol{R}^I_B\big(\dot{\boldsymbol{W}}^B-\delta\boldsymbol{f}^B\big) \tag{39}$$

where $\tilde{\dot{\boldsymbol{W}}}^I$ and $\dot{\boldsymbol{W}}^I$ are the measured and true values of the apparent acceleration expressed in the theory LCI frame, respectively. $\dot{\boldsymbol{W}}^B$ is the output apparent acceleration measured by the accelerometers, and $\delta\boldsymbol{f}^B$ is the accelerometer measurement error.

The quartz accelerometer measurement error model is given by

$$\begin{aligned}\delta\boldsymbol{f}^B&=\begin{bmatrix}E_{0x}+E_{xx}\dot{W}_x+E_{xy}\dot{W}_y+E_{xz}\dot{W}_z\\ E_{0y}+E_{yx}\dot{W}_x+E_{yy}\dot{W}_y+E_{yz}\dot{W}_z\\ E_{0z}+E_{zx}\dot{W}_x+E_{zy}\dot{W}_y+E_{zz}\dot{W}_z\end{bmatrix}+\boldsymbol{\eta}_a\\ &\triangleq\boldsymbol{N}_{acc}\boldsymbol{D}_a+\boldsymbol{\eta}_a\end{aligned} \tag{40}$$

with

$$\boldsymbol{N}_{acc}=\begin{bmatrix}1 & \dot{W}_x & \dot{W}_y & \dot{W}_z & 0 & 0 & 0 & 0 & 0 & 0 & 0 & 0\\ 0 & 0 & 0 & 0 & 1 & \dot{W}_x & \dot{W}_y & \dot{W}_z & 0 & 0 & 0 & 0\\ 0 & 0 & 0 & 0 & 0 & 0 & 0 & 0 & 1 & \dot{W}_x & \dot{W}_y & \dot{W}_z\end{bmatrix} \tag{41}$$

$$\boldsymbol{D}_a=\begin{bmatrix}E_{0x} & E_{xx} & E_{xy} & E_{xz} & E_{0y} & E_{yx} & E_{yy} & E_{yz} & E_{0z} & E_{zx} & E_{zy} & E_{zz}\end{bmatrix}^{\mathrm{T}} \tag{42}$$

where E_{0x}, E_{0y}, E_{0z} are the accelerometer drifts; E_{xx}, E_{yy}, E_{zz} are the scale factors, E_{xy}, E_{xz}, E_{yx}, E_{yz}, E_{zx}, E_{zy} are the misalignments; $\dot{W}_x$, $\dot{W}_y$, $\dot{W}_z$ are the three components of $\dot{\boldsymbol{W}}^B$, respectively. Measurement noise $\boldsymbol{\eta}_a$ is zero-mean Gaussian white-noise processes with spectral densities given by $\sigma^2_a\boldsymbol{I}_{3\times3}$.

By using the error parameter vector $\boldsymbol{K}$, $\delta\boldsymbol{f}^B$ can be rewritten as

$$\delta\boldsymbol{f}^B=\boldsymbol{N}_{df}\boldsymbol{K}+\boldsymbol{\eta}_a \tag{43}$$

with

$$\boldsymbol{N}_{df}=\begin{bmatrix}\boldsymbol{0}_{3\times3} & \boldsymbol{0}_{3\times12} & \boldsymbol{N}_{acc}\end{bmatrix} \tag{44}$$

By using Eq. (10), we obtain

$$\boldsymbol{R}^I_B=\big(\boldsymbol{I}_{3\times3}+[\boldsymbol{\alpha}\times]\big)\boldsymbol{R}^P_B \tag{45}$$

Substituting Eq. (45) into Eq. (39) and neglecting high-order terms gives

$$\begin{aligned}\Delta\dot{\boldsymbol{W}}^I&=\boldsymbol{R}^P_B\dot{\boldsymbol{W}}^B-\big(\boldsymbol{R}^P_B+[\boldsymbol{\alpha}\times]\boldsymbol{R}^P_B\big)\big(\dot{\boldsymbol{W}}^B-\delta\boldsymbol{f}^B\big)\\ &\approx-[\boldsymbol{\alpha}\times]\boldsymbol{R}^P_B\dot{\boldsymbol{W}}^B+\boldsymbol{R}^P_B\delta\boldsymbol{f}^B\\ &=\big[\boldsymbol{R}^P_B\dot{\boldsymbol{W}}^B\times\big]\boldsymbol{\alpha}+\boldsymbol{R}^P_B\delta\boldsymbol{f}^B\end{aligned} \tag{46}$$

Substituting Eqs. (23) and (43) into Eq. (46) leads to

$$\begin{aligned}\Delta\dot{\boldsymbol{W}}^I&=\big\{\big[\boldsymbol{R}^P_B\dot{\boldsymbol{W}}^B\times\big]\boldsymbol{N}_\alpha+\boldsymbol{R}^P_B\boldsymbol{N}_{df}\big\}\boldsymbol{K}+\boldsymbol{R}^P_B\boldsymbol{\eta}_a\\ &\triangleq\boldsymbol{C}_{11}\boldsymbol{K}+\boldsymbol{R}^P_B\boldsymbol{\eta}_a\end{aligned} \tag{47}$$

Integrating Eq. (47) gives the apparent velocity navigation error of strapdown INS

$$\begin{aligned}\Delta\boldsymbol{W}^I&=\int_0^t\big(\boldsymbol{C}_{11}\boldsymbol{K}+\boldsymbol{R}^P_B\boldsymbol{\eta}_a\big)\,dt\approx\int_0^t\boldsymbol{C}_{11}\boldsymbol{K}\,dt\\ &=\int_0^t\boldsymbol{C}_{11}\,dt\,\boldsymbol{K}\triangleq\boldsymbol{C}_{21}\boldsymbol{K}\end{aligned} \tag{48}$$

Taking the integral of Eq. (48) again gives the apparent position navigation error of strapdown INS

$$\Delta \boldsymbol{r}^I = \int_0^t \boldsymbol{C}_{21}\boldsymbol{K}\,dt = \int_0^t \boldsymbol{C}_{21}\,dt\,\boldsymbol{K} \triangleq \boldsymbol{C}_{31}\boldsymbol{K} \tag{49}$$

According to the above analysis, if the gravity computation errors due to the position errors are not taken into consideration, the total velocity navigation errors can be computed by using the initial velocity navigation error and apparent velocity navigation error as

$$\Delta \boldsymbol{v} = \Delta \boldsymbol{v}_0 + \Delta \boldsymbol{W}^I = \boldsymbol{N}_{\boldsymbol{v}_0}\boldsymbol{K} + \boldsymbol{C}_{21}\boldsymbol{K} = (\boldsymbol{N}_{\boldsymbol{v}_0} + \boldsymbol{C}_{21})\boldsymbol{K} \triangleq \boldsymbol{C}_2\boldsymbol{K} \tag{50}$$

And the total position navigation errors can be written as

$$\begin{aligned}\Delta \boldsymbol{r} &= \Delta \boldsymbol{r}_0 + \Delta \boldsymbol{v}_0 t + \Delta \boldsymbol{r}^I = \boldsymbol{N}_{\boldsymbol{r}_0}\boldsymbol{K} + \boldsymbol{N}_{\boldsymbol{v}_0} t\boldsymbol{K} + \boldsymbol{C}_{31}\boldsymbol{K} \\ &= (\boldsymbol{N}_{\boldsymbol{r}_0} + \boldsymbol{N}_{\boldsymbol{v}_0} t + \boldsymbol{C}_{31})\boldsymbol{K} \triangleq \boldsymbol{C}_3\boldsymbol{K}\end{aligned} \tag{51}$$

3.3. Navigation errors caused by gravity computation errors

When performing the navigation computation, the gravitational acceleration $\boldsymbol{g}$ can be expressed in terms of the radial and tangential unit vectors $\boldsymbol{l}_s$ and $\boldsymbol{l}_z$ as follows [17]:

$$\boldsymbol{g} = g_s \boldsymbol{l}_s + g_z \boldsymbol{l}_z \tag{52}$$

where

$$g_s = -\mu/s^2\left[1 + J(a/s)^2\left(1 - 5\sin^2\phi\right)\right],$$

$$g_z = -\left(2\mu/s^2\right)J(a/s)^2\sin\phi,$$

$$\mu = GM = 3.9860322 \times 10^{14}\ \mathrm{m/s^2},$$

J = dimensionless coefficient determined experimentally from satellite observations ($\approx 1.624 \times 10^{-3}$),

ϕ = geodetic latitude,

a = equatorial radius $\quad (= 6{,}378.165\ \mathrm{km})$,

s = distance from the Earth center to the launch vehicle.

Since the navigation position provided by strapdown INS is different from the true position of the launch vehicle, there exist computation errors when using the navigation information to compute the gravitational acceleration. In terms of the definition of navigation errors, the computation errors for the gravitational acceleration caused by the position navigation errors can be represented by

$$\Delta \boldsymbol{g}^I = \boldsymbol{g}\left(\boldsymbol{X}^I + \boldsymbol{\rho}_o^I\right) - \boldsymbol{R}_{I'}^I \boldsymbol{g}\left(\boldsymbol{X}^{I'} + \boldsymbol{\rho}_{o'}^{I'}\right) \tag{53}$$

where $\boldsymbol{X}^I$ is the navigation position vector expressed in the theory LCI frame, $\boldsymbol{X}^{I'}$ is the true position vector expressed in the actual LCI frame, $\boldsymbol{\rho}_o^I$ and $\boldsymbol{\rho}_{o'}^{I'}$ have been defined in the previous subsection.

When analyzing the computation errors of the gravitational acceleration, it is convenient and sufficient to select 2-body gravity model, namely,

$$\boldsymbol{g}(\boldsymbol{s}) = -\frac{\mu}{|\boldsymbol{s}|^3}\boldsymbol{s} \tag{54}$$

Thus, using a Taylor's series expansion and the invariance of the vector length, Eq. (53) can be written as

$$\begin{aligned}\Delta \boldsymbol{g}^I &= \boldsymbol{g}\left(\boldsymbol{X}^I + \boldsymbol{\rho}_o^I\right) - \boldsymbol{g}\left(\boldsymbol{R}_{I'}^I\left(\boldsymbol{X}^{I'} + \boldsymbol{\rho}_{o'}^{I'}\right)\right) \\ &= \left.\frac{\partial \boldsymbol{g}}{\partial \boldsymbol{s}}\right|_{(\boldsymbol{X}^I + \boldsymbol{\rho}_o^I)}\left[\left(\boldsymbol{X}^I + \boldsymbol{\rho}_o^I\right) - \boldsymbol{R}_{I'}^I\left(\boldsymbol{X}^{I'} + \boldsymbol{\rho}_{o'}^{I'}\right)\right] \\ &= \left.\frac{\partial \boldsymbol{g}}{\partial \boldsymbol{s}}\right|_{(\boldsymbol{X}^I + \boldsymbol{\rho}_o^I)}\left[\left(\boldsymbol{X}^I - \boldsymbol{R}_{I'}^I\boldsymbol{X}^{I'}\right) + \left(\boldsymbol{\rho}_o^I - \boldsymbol{R}_{I'}^I\boldsymbol{\rho}_{o'}^{I'}\right)\right]\end{aligned} \tag{55}$$

with

$$\frac{\partial \boldsymbol{g}}{\partial \boldsymbol{s}} = -\frac{\mu}{|\boldsymbol{s}|^3}\left(\boldsymbol{I}_{3\times 3} - 3\hat{\boldsymbol{s}}\hat{\boldsymbol{s}}^{\mathrm{T}}\right) \tag{56}$$

where $\hat{\boldsymbol{s}}$ is the unit vector of $\boldsymbol{s}$.

By the definitions, the variables in the square bracket on the right side of Eq. (55) are essentially the total position navigation errors. Thus, using Eq. (51), Eq. (55) can be rewritten as

$$\Delta \boldsymbol{g}^I = \left.\frac{\partial \boldsymbol{g}}{\partial \boldsymbol{s}}\right|_{(\boldsymbol{X}^I + \boldsymbol{\rho}_o^I)}\Delta \boldsymbol{r} = \left.\frac{\partial \boldsymbol{g}}{\partial \boldsymbol{s}}\right|_{(\boldsymbol{X}^I + \boldsymbol{\rho}_o^I)}\boldsymbol{C}_3\boldsymbol{K} \triangleq \boldsymbol{C}_{12}\boldsymbol{K} \tag{57}$$

The velocity and position navigation errors caused by $\Delta \boldsymbol{g}^I$ are given by

$$\Delta \boldsymbol{v}_g = \int_0^t \boldsymbol{C}_{12}\boldsymbol{K}\,dt = \int_0^t \boldsymbol{C}_{12}\,dt\,\boldsymbol{K} \triangleq \boldsymbol{C}_{22}\boldsymbol{K} \tag{58}$$

$$\Delta \boldsymbol{r}_g = \int_0^t \boldsymbol{C}_{22}\boldsymbol{K}\,dt = \int_0^t \boldsymbol{C}_{22}\,dt\,\boldsymbol{K} \triangleq \boldsymbol{C}_{32}\boldsymbol{K} \tag{59}$$

Therefore, with the consideration of the gravity computation errors due to the position navigation errors, the total velocity and position navigation errors in Eqs. (50) and (51) can be rewritten as

$$\Delta \boldsymbol{v} = \Delta \boldsymbol{v}_0 + \Delta \boldsymbol{W}^I + \Delta \boldsymbol{v}_g = (\boldsymbol{N}_{\boldsymbol{v}_0} + \boldsymbol{C}_{21} + \boldsymbol{C}_{22})\boldsymbol{K} \triangleq \boldsymbol{C}_2\boldsymbol{K} \tag{60}$$

$$\begin{aligned}\Delta \boldsymbol{r} &= \Delta \boldsymbol{r}_0 + \Delta \boldsymbol{v}_0 t + \Delta \boldsymbol{r}^I + \Delta \boldsymbol{r}_g \\ &= (\boldsymbol{N}_{\boldsymbol{r}_0} + \boldsymbol{N}_{\boldsymbol{v}_0} t + \boldsymbol{C}_{31} + \boldsymbol{C}_{32})\boldsymbol{K} \triangleq \boldsymbol{C}_3\boldsymbol{K}\end{aligned} \tag{61}$$

It follows from Eq. (57) that the matrix $\boldsymbol{C}_3$ is required for the calculation of $\Delta \boldsymbol{g}^I$. The previous-time $\boldsymbol{C}_3$ computed by Eq. (61) is used to calculate the Eq. (57). It is straightforwardly seen from Eq. (61) that the initial value of $\boldsymbol{C}_3$ is equal to $\boldsymbol{N}_{\boldsymbol{r}_0}$. At this moment, Eq. (57) is essentially used to calculate the gravity acceleration computation errors caused by the initial position navigation error, which agrees with the actual situation. Consequently, it can be shown that the gravity computation errors due to the total position navigation errors can be approximately compensated using this method. It is noted that the forward Euler's integration method is used to calculate the above function matrices. The integration step coincides with the navigation computation step.

4. Estimation of error parameters

In this section, a dual star correction strategy scheme is presented to estimate the error parameter vector $\boldsymbol{K}$ and correct the cumulative velocity and position navigation errors. As shown in Fig. 3, the detailed scheme is summarized as follows:

Step 1: When the main engines shut down, the digital platform misalignment angle $\hat{\boldsymbol{\alpha}}_k$ (includes $\boldsymbol{\alpha}_\Delta$ and $\boldsymbol{\alpha}_g$) at shut down time t_k is determined using the attitude information measured by the star sensor, and then fed into the Kalman filter as the initial state value.

Step 2: The gyro error coefficients $\hat{\boldsymbol{D}}_g$ and the current digital platform misalignment angle $\hat{\boldsymbol{\alpha}}$ are estimated by the designed Kalman filter. The stellar update procedure is accomplished by using the estimated digital platform misalignment angle and INS

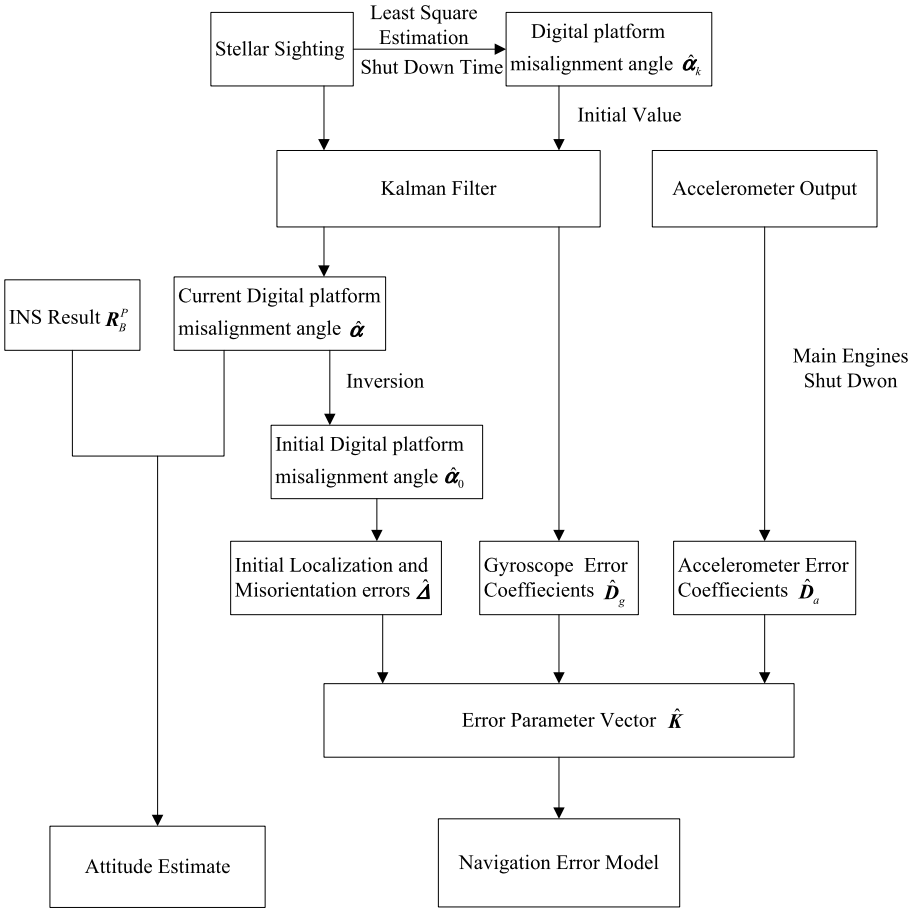

Fig. 3. The workflow of dual star correction strategy scheme.

navigation result $\boldsymbol{R}_B^P$. The inversion of initial digital platform misalignment angle $\hat{\boldsymbol{\alpha}}_0$ (only includes $\boldsymbol{\alpha}_\Delta$) is performed by using the state transition matrix. Subsequently, the initial localization and misorientation errors $\hat{\boldsymbol{\Delta}}$ can be estimated by using Eq. (7).

Step 3: The drift errors of the accelerometers are estimated by using the accelerometer output in the post-boost phase, and other accelerometer error coefficients are assigned as zero. Thus, we obtain the estimates of the accelerometer error coefficients $\hat{\boldsymbol{D}}_a$.

Step 4: The estimates for $\hat{\boldsymbol{\Delta}}$, $\hat{\boldsymbol{D}}_g$ and $\hat{\boldsymbol{D}}_a$ are concatenated to form the error parameter vector $\hat{\boldsymbol{K}}$, which is then fed into the navigation error model to correct the cumulative velocity and position navigation errors.

4.1. The least squares estimation of digital platform misalignment angle at shut down time

Although the star sensor can work as soon as the vehicle flies off the atmosphere, the stellar sighting is usually made after the end of the main engines burn out. This is because the rotation of the vehicle for the sighting will affect the control stabilization of the vehicle before the main engines burn out and the engine oscillation also will affect the accuracy of the star sensor. For a strapdown stellar-inertial system, the stabilization of the star sensor line of sight can be performed by strict control of the vehicle motion during the sighting, or by allowing limited degrees of freedom of the strapdown cluster during the sighting [11].

The measurement model of the star sensor is given by [21]

$$\boldsymbol{S}^B = \boldsymbol{R}_I^B \boldsymbol{S}^I + \boldsymbol{\eta}_s \tag{62}$$

where $\boldsymbol{S}^B$ is the unit vector of navigation star measured in the body frame, $\boldsymbol{S}^I$ is the corresponding unit vector expressed in the theory LCI frame. The sensor measurement noise $\boldsymbol{\eta}_s$ is approximately Gaussian which satisfies

$$E\{\boldsymbol{\eta}_s\} = \boldsymbol{0} \tag{63}$$

$$E\{\boldsymbol{\eta}_s \boldsymbol{\eta}_s^{\mathrm{T}}\} = \sigma_s^2\left[\boldsymbol{I}_{3\times 3} - \left(\boldsymbol{R}_I^B \boldsymbol{S}^I\right)\left(\boldsymbol{R}_I^B \boldsymbol{S}^I\right)^{\mathrm{T}}\right] \tag{64}$$

and $E\{\cdot\}$ denotes expectation. Eq. (64) is known as the QUEST measurement model which is quite accurate for small field-of-view sensors. The advantage of using the model is that the measurement covariance matrix in the EKF formulation can effectively be replaced by a nonsingular matrix given by $\sigma_s^2 \boldsymbol{I}_{3\times 3}$ [14,13].

By using the attitude transformation relationship and Eq. (1), Eq. (62) can be rewritten as

$$\boldsymbol{S}^B = \boldsymbol{R}_P^B \boldsymbol{R}_I^P \boldsymbol{S}^I + \boldsymbol{\eta}_s = \boldsymbol{R}_P^B\left(\boldsymbol{I}_{3\times 3} - [\boldsymbol{\alpha}\times]\right)\boldsymbol{S}^I + \boldsymbol{\eta}_s \tag{65}$$

Rearranging Eq. (65) leads to

$$\boldsymbol{R}_B^P \boldsymbol{S}^B - \boldsymbol{S}^I = \left[\boldsymbol{S}^I\times\right]\boldsymbol{\alpha} + \boldsymbol{\eta}_s \tag{66}$$

Hence, two star sensor vector measurements can be concatenated to form

$$\boldsymbol{Y}_\alpha = \boldsymbol{H}_\alpha \boldsymbol{\alpha} + \boldsymbol{\eta}_s \tag{67}$$

with

$$\boldsymbol{Y}_\alpha = \begin{pmatrix} \boldsymbol{R}_B^P \boldsymbol{S}_1^B - \boldsymbol{S}_1^I \\ \boldsymbol{R}_B^P \boldsymbol{S}_2^B - \boldsymbol{S}_2^I \end{pmatrix} \qquad \boldsymbol{H}_\alpha = \begin{pmatrix} [\boldsymbol{S}_1^I\times] \\ [\boldsymbol{S}_2^I\times] \end{pmatrix} \qquad \boldsymbol{\eta}_s = \begin{pmatrix} \boldsymbol{\eta}_{s1} \\ \boldsymbol{\eta}_{s2} \end{pmatrix} \tag{68}$$

The least squares estimation of the digital platform misalignment angle at shut down time t_k is given by

$$\hat{\boldsymbol{\alpha}}_k = \left(\boldsymbol{H}_\alpha^{\mathrm{T}}\boldsymbol{H}_\alpha\right)^{-1}\boldsymbol{H}_\alpha^{\mathrm{T}}\boldsymbol{Y}_\alpha \tag{69}$$

4.2. The estimation of gyro error coefficients and initial localization and misorientation errors

It follows from the preceding analysis that the initial digital platform errors caused by the initial localization and misorientation errors don't change with time. Therefore, taking the time derivative of Eq. (17) or using Eqs. (15) and (18) leads to

$$\begin{aligned}\dot{\boldsymbol{\alpha}} &= -\boldsymbol{R}_B^I(\boldsymbol{N}_{gyro}\boldsymbol{D}_g + \boldsymbol{\eta}_\omega)\\ &= -\left(\boldsymbol{I}_{3\times3} + [\boldsymbol{\alpha}\times]\right)\boldsymbol{R}_B^P(\boldsymbol{N}_{gyro}\boldsymbol{D}_g + \boldsymbol{\eta}_\omega)\end{aligned} \tag{70}$$

Based upon the state dynamics and observations Eqs. (70) and (67), the extended Kalman filter (EKF) model can be written with $\boldsymbol{X}_\alpha = [\boldsymbol{\alpha}^{\mathrm{T}}\ \boldsymbol{D}_g^{\mathrm{T}}]^{\mathrm{T}}$ and $\boldsymbol{w} = \boldsymbol{\eta}_\omega$ as

$$\begin{cases}\dot{\boldsymbol{X}}_\alpha = \boldsymbol{F}_\alpha\boldsymbol{X}_\alpha + \boldsymbol{G}\boldsymbol{w}\\ \boldsymbol{Y}_\alpha = \boldsymbol{H}'_\alpha\boldsymbol{X}_\alpha + \boldsymbol{\eta}_s\end{cases} \tag{71}$$

where

$$\boldsymbol{F}_\alpha = \begin{bmatrix}[(\boldsymbol{R}_B^P\boldsymbol{N}_{gyro}\hat{\boldsymbol{D}}_g)\times] & -(\boldsymbol{I}_{3\times3} + [\hat{\boldsymbol{\alpha}}\times])\boldsymbol{R}_B^P\boldsymbol{N}_{gyro}\\ \boldsymbol{0}_{12\times3} & \boldsymbol{0}_{12\times12}\end{bmatrix} \tag{72}$$

$$\boldsymbol{G} = \begin{bmatrix}-(\boldsymbol{I}_{3\times3} + [\hat{\boldsymbol{\alpha}}\times])\boldsymbol{R}_B^P\\ \boldsymbol{0}_{12\times3}\end{bmatrix} \tag{73}$$

$$\boldsymbol{H}'_\alpha = [\ \boldsymbol{H}_\alpha \quad \boldsymbol{0}_{6\times12}\ ] \tag{74}$$

The aforementioned Kalman filter operates during the period between the end of the main engines burn and the start of the reentry phase. From time t_k, the gyro error coefficients $\boldsymbol{D}_g$ and the current digital platform misalignment angle $\boldsymbol{\alpha}$ are estimated by using Eq. (71), and the initial state value is $\boldsymbol{X}_\alpha(0) = [\hat{\boldsymbol{\alpha}}_k^{\mathrm{T}}\ \boldsymbol{0}_{1\times12}]^{\mathrm{T}}$. For the sake of brevity, the well-known Kalman filtering equations which can be easily found in [9] are not repeated here. Therefore, the stellar update procedure is accomplished by the implementation of the estimated total misalignment angles $\boldsymbol{\alpha}$ and the navigation computation result $\boldsymbol{R}_B^P$ using the following expression

$$\hat{\boldsymbol{R}}_B^I = \left(\boldsymbol{I}_{3\times3} + [\hat{\boldsymbol{\alpha}}\times]\right)\boldsymbol{R}_B^P \tag{75}$$

In addition, the recursion computation for the transition matrix of $\boldsymbol{F}_\alpha$ can be described as

$$\begin{cases}\boldsymbol{\Phi}(t_n, t_{n-1}) \approx I + \boldsymbol{F}_\alpha\Delta t + \boldsymbol{F}_\alpha^2\Delta t^2/2 + \boldsymbol{F}_\alpha^3\Delta t^3/6\\ \boldsymbol{\Phi}(t_n, t_0) = \boldsymbol{\Phi}(t_n, t_{n-1})\cdots\boldsymbol{\Phi}(t_k, t_{k-1})\boldsymbol{\Phi}(t_2, t_1)\boldsymbol{\Phi}(t_1, t_0)\end{cases} \tag{76}$$

where $\boldsymbol{\Phi}(t_n, t_{n-1})$ is the state transition matrix from time t_{n-1} to time t_n, Δt is the sampling interval and $t_0 = 0$. Since the Kalman filter has not started to work before the main engines shut down, it should be noted that the estimates for $\hat{\boldsymbol{\alpha}}$ and $\hat{\boldsymbol{D}}_g$ which are used to compute coefficient matrix $\boldsymbol{F}_\alpha$ during the boost phase (i.e., from time t_0 to shut down time t_k) are zero. From shut down time t_k to current time t_n ($t_n > t_k$), the estimates for $\hat{\boldsymbol{\alpha}}$ and $\hat{\boldsymbol{D}}_g$ which are used to compute coefficient matrix $\boldsymbol{F}_\alpha$ are determined by the designed Kalman filter. Then, the state transition matrix $\boldsymbol{\Phi}(t_n, t_0)$ from time t_0 to current time t_n can be recursively calculated by using Eq. (76).

Thus, the estimate of the initial digital platform misalignment angle $\hat{\boldsymbol{\alpha}}_0$ can be obtained in turn by

$$\left.\begin{bmatrix}\hat{\boldsymbol{\alpha}}\\ \hat{\boldsymbol{D}}_g\end{bmatrix}\right|_{t=t_0} = \boldsymbol{\Phi}^{-1}(t_n, t_0)\left.\begin{bmatrix}\hat{\boldsymbol{\alpha}}\\ \hat{\boldsymbol{D}}_g\end{bmatrix}\right|_{t=t_n} \tag{77}$$

where the estimates for $\hat{\boldsymbol{\alpha}}$ and $\hat{\boldsymbol{D}}_g$ at current time t_n are determined by Kalman filter in real. Therefore, the initial digital platform misalignment angle $\hat{\boldsymbol{\alpha}}_0$ can be continuously estimated as the Kalman filter works. It follows from the analysis of the digital platform errors in Section 2 that the initial digital platform misalignment angle $\hat{\boldsymbol{\alpha}}_0$ is merely caused by the initial localization and misorientation errors. Up to this point, the initial localization and misorientation errors can be estimated by

$$\hat{\boldsymbol{\Delta}} = \boldsymbol{N}_\Delta^{-1}\hat{\boldsymbol{\alpha}}_0 \tag{78}$$

4.3. The estimation of accelerometer error coefficients

When the main engines shut down, the thrust and atmosphere drag are assumed to be zero. Consequently, it follows from Eq. (40) that the accelerometer output is statistically the drift errors of the accelerometers, namely,

$$\begin{bmatrix}\hat{E}_{0x}\\ \hat{E}_{0y}\\ \hat{E}_{0z}\end{bmatrix} = \frac{1}{n-k+1}\sum_{j=k}^{n}\left(\delta\boldsymbol{f}^B\right)_j = \frac{1}{n-k+1}\sum_{j=k}^{n}\left(\dot{\boldsymbol{W}}^B\right)_j \tag{79}$$

where k and n are the shut down and current time sequences, respectively. Obviously, Eq. (79) can be expressed as the following recursive form

$$\left.\begin{bmatrix}\hat{E}_{0x}\\ \hat{E}_{0y}\\ \hat{E}_{0z}\end{bmatrix}\right|_{n+1} = \frac{n-k+1}{n-k+2}\left.\begin{bmatrix}\hat{E}_{0x}\\ \hat{E}_{0y}\\ \hat{E}_{0z}\end{bmatrix}\right|_{n} + \frac{1}{n-k+2}\left(\dot{\boldsymbol{W}}^B\right)_{n+1} \tag{80}$$

Since the stellar sighting cannot be used to correct the accelerometer error coefficients, Eq. (80) is used to estimate the drift errors of the accelerometers. In general, the drift errors are the primary error factors in the accelerometer error model. Unfortunately, the scale factors and misalignments of the accelerometers cannot be estimated by using the integrated sensor system of this paper. With the consideration of the small magnitude of these error coefficients, the scale factors and misalignments are approximately estimated with zero. Thus, we obtain the estimates of the accelerometer error coefficients as follows

$$\hat{\boldsymbol{D}}_a = \left[\ \hat{E}_{0x}\quad \boldsymbol{0}_{1\times3}\quad \hat{E}_{0y}\quad \boldsymbol{0}_{1\times3}\quad \hat{E}_{0z}\quad \boldsymbol{0}_{1\times3}\ \right]^{\mathrm{T}} \tag{81}$$

Then, the estimate of the error parameter vector $\boldsymbol{K}$ can be written as

$$\hat{\boldsymbol{K}} = \left[\ \hat{\boldsymbol{\Delta}}^{\mathrm{T}}\quad \hat{\boldsymbol{D}}_g^{\mathrm{T}}\quad \hat{\boldsymbol{D}}_a^{\mathrm{T}}\ \right] \tag{82}$$

Finally, the cumulative velocity and position navigation errors can be estimated and compensated by substituting Eq. (82) into Eqs. (60) and (61).

5. Simulation results and analysis

In this section, simulation results are presented that analyze the effects of the individual error factor with respect to strapdown INS and show the performance of the proposed stellar-inertial integrated navigation scheme. For the simulation examples a launch vehicle is considered that has a three-axis optic fiber gyro and a three-axis quartz accelerometer as well as a star sensor. It is assumed that two stars are available for stellar sighting during the entire simulation and the reference stars are selected from the Tycho-2 Star Catalog. A rocket motion time history including the boosted flight time of 180 s and the free-all time of 300 s has been used in the test cases. The total simulation time is 480 s.

The basic simulation parameters used in the test cases are:

(1) The nominal launch azimuth, latitude and longitude: $A_0 = 10.208°$, $B_0 = 40°$, $\lambda_0 = 99°$;

Table 1
The effects of the individual error factor with respect to strapdown INS.

Nominal accuracy initial launching parameter errors and inertial sensor drift errors $\boldsymbol{\Delta} = [50'' \ 20'' \ 20'']^{\mathrm{T}}$, $D_{0x} = D_{0y} = D_{0z} = 0.05^\circ/\mathrm{h}$, $E_{0x} = E_{0y} = E_{0z} = 1 \times 10^{-4}$ m/s^2						
Error source	δv_x (m·s^{-1})	δv_y (m·s^{-1})	δv_z (m·s^{-1})	δx (m)	δy (m)	δz (m)
Initial localization and misorientation errors $\boldsymbol{\Delta}$	0.12	0.54	1.54	−722.5	203.4	179.1
Gyro measurement error $\delta \boldsymbol{\omega}_{B/I}^{B}$	−0.02	0.12	−0.13	−14.4	35.0	−48.9
Accelerometer measurement error $\delta \boldsymbol{f}^{B}$	0.06	0.10	0.12	13.3	37.4	38.4
Total	0.16	0.76	1.53	−723.6	275.8	168.7
Low accuracy initial launching parameter errors and inertial sensor drift errors $\boldsymbol{\Delta} = [-180'' \ 50'' \ 50'']^{\mathrm{T}}$, $D_{0x} = D_{0y} = D_{0z} = 0.5^\circ/\mathrm{h}$, $E_{0x} = E_{0y} = E_{0z} = 1 \times 10^{-3}$ m/s^2						
Error source	δv_x (m·s^{-1})	δv_y (m·s^{-1})	δv_z (m·s^{-1})	δx (m)	δy (m)	δz (m)
Initial localization and misorientation errors $\boldsymbol{\Delta}$	0.32	1.37	5.14	−1805.5	509.1	915.6
Gyro measurement error $\delta \boldsymbol{\omega}_{B/I}^{B}$	−0.30	1.76	−2.11	−162.2	551.4	−771.6
Accelerometer measurement error $\delta \boldsymbol{f}^{B}$	0.40	0.14	0.52	83.9	70.0	139.4
Total	0.42	3.27	3.55	−1883.6	1130.5	283.4

Table 2
Navigation performance comparisons for three types of guidance schemes.

Guidance scheme	δv_x (m·s^{-1})	δv_y (m·s^{-1})	δv_z (m·s^{-1})	δx (m)	δy (m)	δz (m)
All-inertial	0.16	0.76	1.53	−723.6	275.8	168.7
Stellar-inertial	0.47	0.06	0.17	58.3	29.5	66.4
Stellar-inertial + gravity compensation	0.03	0.08	0.05	−50.3	30.8	21.0

(2) Optic fiber gyro: scale factors $D_{xx} = D_{yy} = D_{zz} = 1 \times 10^{-5}$, misalignments $D_{xy} = D_{xz} = D_{yx} = D_{yz} = D_{zx} = D_{zy} = 1 \times 10^{-5}$ rad, measurement noise $\sigma_\omega = 2.4 \times 10^{-7}$ rad/$\sqrt{\mathrm{s}}$, sample rate 50 Hz;

(3) Quartz accelerometer: scale factors $E_{xx} = E_{yy} = E_{zz} = 1 \times 10^{-5}$, misalignments $E_{xy} = E_{xz} = E_{yx} = E_{yz} = E_{zx} = E_{zy} = 1 \times 10^{-5}$ rad, measurement noise $\sigma_a = 2.0 \times 10^{-4}$ (m/s)/$\sqrt{\mathrm{s}}$, sample rate 50 Hz;

(4) Star sensor: measurement standard deviation $\sigma_s = 10''$, sample rate 1 Hz.

5.1. Effect analysis of individual error factor

As mentioned above, there are three primary error factors resulting in the velocity and position navigation errors. They are the initial localization and misorientation errors, gyro measurement error and accelerometer measurement error, respectively. In this test case three scenario simulations have been performed to analyze the effects of the individual error factor with respect to the accuracy of strapdown INS. In each scenario only one type of error source is added and the simulation results are summarized in Table 1. Nominal accuracy and low accuracy initial launching parameter errors and inertial sensor drift errors are investigated.

As it is shown in Table 1, the velocity and position navigation errors due to the initial localization and misorientation errors are much larger than those due to the inertial sensor errors. Since the flight time is not long, the effects of the inertial sensor errors are not large and thus the initial launching parameter errors are the primary error factors resulting in the navigation errors. In fact, from the discussions in Section 2, we can conclude that the navigation errors due to the initial localization and misorientation errors are divided into two parts. As the nominal accuracy test case an example, the initial position and velocity navigation errors caused by $\boldsymbol{\Delta}$ are $\Delta \boldsymbol{r}_0 = [-691.2 \quad 0.05 \quad -357.5]^{\mathrm{T}}$ and $\Delta \boldsymbol{v}_0 = [-0.02 \quad 0.02 \quad 0.03]^{\mathrm{T}}$, respectively. From Table 1, we can clearly see that there are velocity and position navigation errors of another part caused by $\boldsymbol{\Delta}$. This is because the initial localization and misorientation errors cause the digital platform errors, and the digital platform errors of this part cause the navigation errors, which is consistent with the previous analysis. The navigation errors of this part increase with fight time, and the magnitudes are large, especially for the velocity.

Compared with the nominal accuracy and low accuracy examples, we find that the effects of the initial localization and misorientation errors with respect to strapdown INS are very large. In addition, it can be seen that the navigation errors due to gyro measurement error become dramatically large when the gyros degrade, while the navigation errors due to the accelerometer measurement error are still likely to be acceptable when the accelerometers degrade. This is because the gyro measurement error causes the digital platform errors, and the effects of the digital platform errors with respect to strapdown INS are more significant than the accelerometer measurement error. Therefore, in order to improve strapdown INS accuracy, it is very necessary to decrease the initial localization and misorientation uncertainties and improve the gyro measurement accuracy.

5.2. Performance comparisons of guidance schemes

There are three types of guidance schemes used in the following numerical examples: all-inertial, stellar-inertial, and stellar-inertial plus the gravity compensation. Notice that the stellar-inertial guidance scheme herein is referred to as the stellar update scheme without the consideration of the compensation for the gravity computation errors. The objective of this test case is to verify the effectiveness of the proposed stellar update scheme and the compensation scheme for the gravity computation errors.

The basic simulation parameters used in this test case have been described in the previous section, and the nominal accuracy initial launching parameter errors and inertial sensor errors are used. The navigation performance comparisons for three types of guidance schemes are given in Table 2. It is clear from this table that the stellar-inertial guidance scheme can compensate the cumulative velocity and position navigation errors effectively. From the simulation results, we can see that the proposed algorithm gives a good estimate for the initial launching parameter errors.

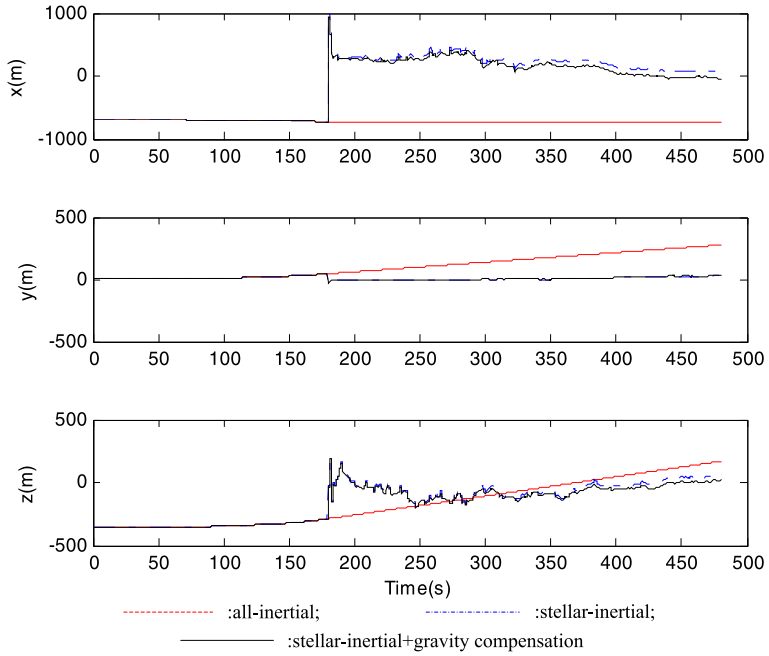

Fig. 4. Position navigation errors for the three types of guidance schemes.

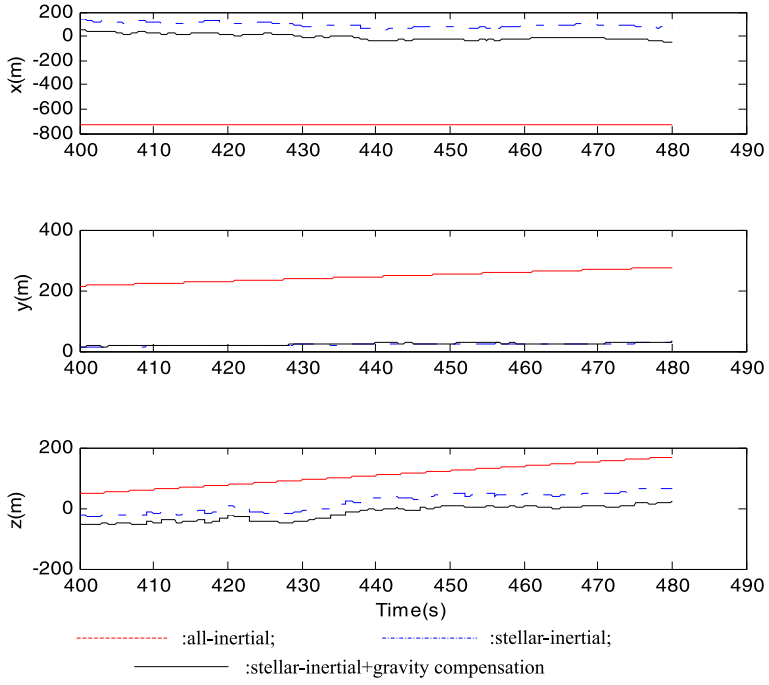

Fig. 5. Partial enlargement drawing of position navigation errors.

In another word, the sensitivity to initial localization and misorientation errors for stellar-inertial system is much lower than that for all-inertial system. This is because launch latitude and longitude errors represent not translational errors but rotational errors around the earth, and the star sensor is capable of minimizing the effects of rotational errors. Compared with the stellar-inertial and stellar-inertial plus gravity compensation systems, we can see that the latter system offers a better accuracy. This implies the gravity compensation scheme can provide an effective correction for the navigation errors, particular for the velocity navigation errors. The position and velocity navigation errors for the three types of guidance schemes as well as their partial enlargement drawing are illustrated in Figs. 4–7. The attitude estimation results for all-inertial and stellar-inertial guidance schemes are plotted in Fig. 8. The attitude estimate errors for the stellar-inertial guidance scheme are within 1×10^{-4} degrees.

6. Conclusions

A computationally efficient dual-star stellar-inertial guidance scheme with the consideration of the gravity computation errors due to the position navigation errors has been designed to estimate the error parameters and correct the velocity and position navigation errors. The detailed mathematical models for the digital platform errors and navigation errors caused by the initial localization and misorientation errors and inertial sensor errors are

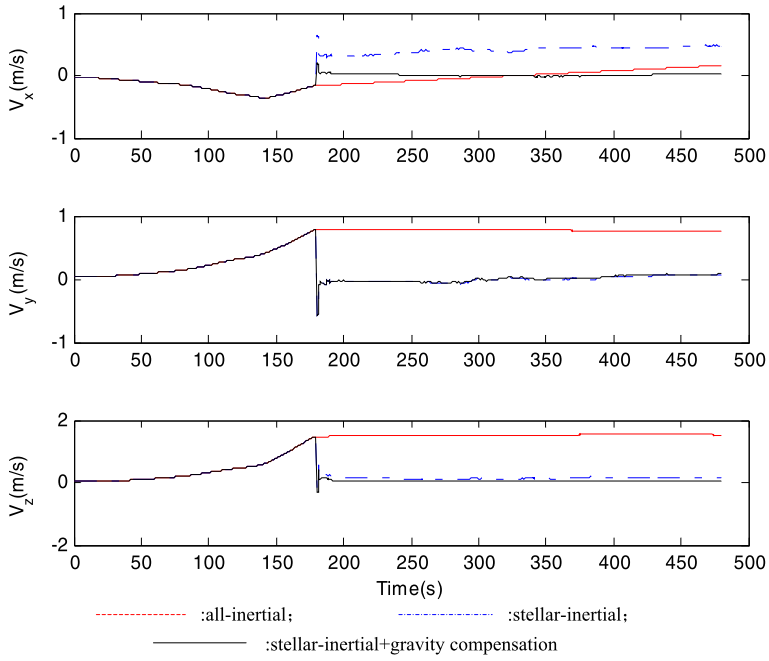

Fig. 6. Velocity navigation errors for the three types of guidance schemes.

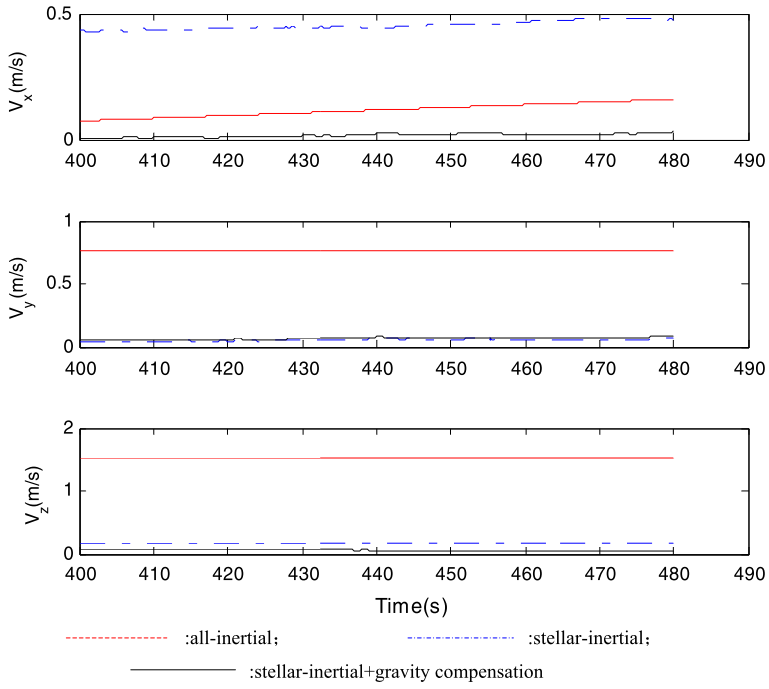

Fig. 7. Partial enlargement drawing of velocity navigation errors.

derived. For the gravity computation errors due to the position errors, an effective first-order approximation compensation scheme is addressed. Compared with traditional stellar-inertial guidance algorithm based on nominal trajectory data and priori subsystem error statistics, the proposed algorithm has the advantages of higher precision and needless selection of optimal stellar sighting direction. Simulation results indicate that the prelaunch position and azimuth errors are the primary error factors resulting in the navigation errors among others, and the proposed stellar-inertial plus gravity compensation guidance scheme can provide the accurate corrections for the velocity and position navigation errors.

Acknowledgements

The authors are grateful to the associate editor and anonymous reviewers for their helpful suggestions and remarks. This work was supported by Innovation Fund of Graduate Program of National University of Defense Technology (B130105) and Scientific Research Fund of Graduate Program of Hunan Province (CX2013B004).

References

[1] K.K. Brown, Is operationally responsive space the future of access to space for the US air force, Air & Space Power Journal 20 (2) (2006) 11–18.

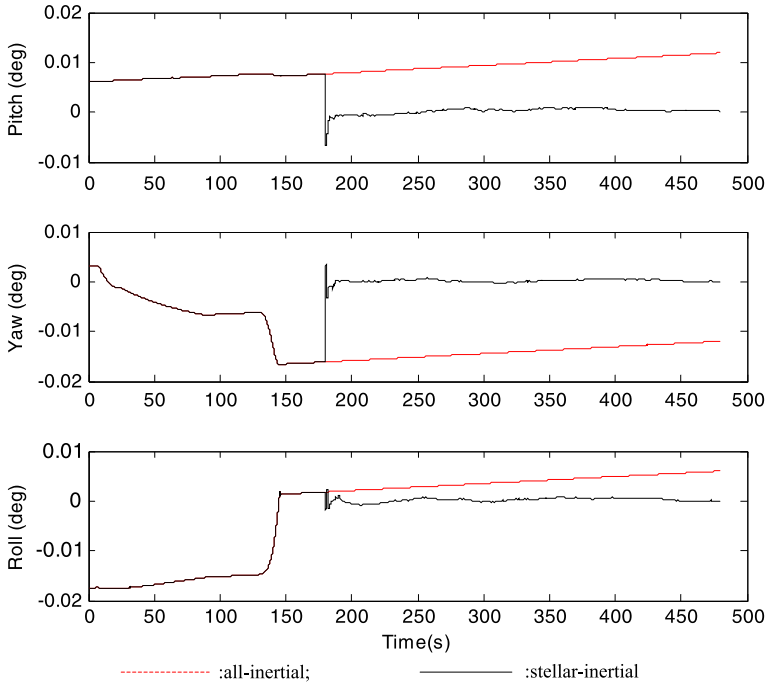

Fig. 8. Attitude estimate errors for all-inertial and stellar-inertial guidance schemes.

[2] S. Chen, L. Li, Design of Control System, Astronautic Press, Beijing, 1996, pp. 233–292.
[3] J.L. Crassidis, Sigma-point Kalman filtering for integrated GPS and inertial navigation, in: Collection of Technical Papers – AIAA Guidance, Navigation, and Control Conference, San Francisco, CA, United States, 2005, pp. 1981–2004.
[4] Z. Fan, Current state of the development of star light inertial guidance technology and performance analysis, National Air Intelligence Center, ADA310487, 1996.
[5] R.V. Gates, M.G. Hall, SLBM fire control computational algorithms in support of stellar inertial guidance, AD A090650, 1980.
[6] S.P. Kau, S.S. Steadman, Update strategy for a strapdown stellar-inertial navigation system, in: Conference on Decision and Control and Symposium on Adaptive Processes, Clearwater, 1976, pp. 58–64.
[7] B. Lichtenstein, Testing of stellar-inertial guidance systems, IEEE Transactions on Military Electronics 7 (1) (1963) 29–35.
[8] R. Linares, J.L. Crassidis, P. Singla, On-orbit gyro calibration for operationally responsive space systems, in: AIAA/AAS Astrodynamics Specialist Conference, Toronto, Ontario Canada, 2010, AIAA 2010-7517.
[9] P.S. Maybeck, Stochastic Models, Estimation, and Control, vol. 2, Navtech Book and Software Store, Arlington, VA, 1994.
[10] S. Nassar, N. El-Sheimy, A combined algorithm on improving INS error modeling and sensor measurements for accurate INS/GPS navigation, GPS Solutions 10 (2006) 29–39.
[11] S.F. Rounds, G. Marmar, Stellar-inertial guidance capability for advanced ICBM, in: Guidance and Control Conference, Gatlinburg, TN, 1983, pp. 849–885.
[12] P.G. Savage, Strapdown inertial navigation integration algorithm design Part 2: velocity and position algorithms, Journal of Guidance, Control and Dynamics 21 (2) (1998) 208–211.
[13] M.D. Shuster, Maximum likelihood estimation of spacecraft attitude, The Journal of the Astronautical Sciences 37 (1) (1989) 79–88.
[14] M.D. Shuster, Kalman filtering of spacecraft attitude and the QUEST model, The Journal of the Astronautical Sciences 38 (3) (1990) 377–393.
[15] M.D. Shuster, A survey of attitude representations, Journal of the Astronautical Sciences 41 (4) (1993) 439–517.
[16] M.D. Shuster, S.D. Oh, Three-axis attitude determination from vector observations, Journal of Guidance and Control 4 (1) (1981) 70–77.
[17] G.M. Siouris, Aerospace Avionics System: A Modern Synthesis, Academic Press, New York, 1993.
[18] G.M. Siouris, Missile Guidance and Control Systems, Springer, 2003.
[19] D.H. Titterton, J.L. Weston, Strapdown Inertial Navigation Technology, The Institution of Electrical Engineers Press, 1997.
[20] R.L. Topping, Submarine launched ballistic missile – improved accuracy, in: AIAA Annual Meeting and Technical Display on Frontiers of Achievement, Long Beach, CA, May 1981.
[21] G. Wahba, A least squares estimate of spacecraft attitude, SIAM Review 7 (3) (1965) 409–411.
[22] X. Wang, J. Xie, L. Guo, A study on Model of strapdown inertial/starlight integrated guidance system for ballistic missiles, Journal of Ballistics 20 (3) (2008) 87–91.
[23] F. Xu, J. Fang, Velocity and position error compensation using strapdown inertial navigation system/celestial navigation system in integration based on ensemble neural network, Aerospace Science and Technology 12 (4) (2008) 302–307.
[24] H. Zhang, W. Zheng, G. Tang, Stellar/inertial integrated guidance for responsive launch vehicles, Aerospace Science and Technology 18 (1) (2012) 35–41.
[25] H. Zhang, W. Zheng, J. Wu, G. Tang, Investigation on single-star stellar-inertial guidance principle using equivalent formation compression theory, Science in China, Series E: Technological Sciences 52 (10) (2009) 2924–2929.